International Journal of Remote Sensing
Vol. 32, No. 21, 10 November 2011, 6071–6089

Histogram thresholding for unsupervised change detection of remote sensing images

SWARNAJYOTI PATRA†, SUSMITA GHOSH† and ASHISH GHOSH*‡
†Department of Computer Science and Engineering, Jadavpur University, Kolkata 700032, India
‡Center for Soft Computing Research, Indian Statistical Institute, Kolkata 700108, India

(*Received 4 November 2009; in final form 5 July 2010*)

The change-detection problem can be viewed as an unsupervised classification problem with two classes corresponding to changed and unchanged areas. Image differencing is a widely used approach to change detection. It is based on the idea of generating a difference image that represents the modulus of the spectral change vectors associated with each pixel in the study area. To separate out the changed and unchanged classes in the difference image automatically, any unsupervised technique can be used. Thresholding is one of the cheapest techniques among them. However, in thresholding approaches, selection of the best threshold value is not a trivial task. In this work, several non-fuzzy and fuzzy histogram thresholding techniques are investigated and compared for the change-detection problem. Experimental results, carried out on different multitemporal remote sensing images (acquired before and after an event), are used to assess the effectiveness of each of the thresholding techniques. Among all the thresholding techniques investigated here, Liu's fuzzy entropy followed by Kapur's entropy are found to be the most robust techniques.

1. Introduction

In remote sensing applications, change detection is the process of identifying differences in the state of an object or phenomenon by analysing a pair of images acquired on the same geographical area at two different instants (Singh 1989). Such a problem plays an important role in various domains, like studies on land-use/land-cover dynamics (Cihlar *et al.* 1992), monitoring shifting cultivations (Bruzzone and Serpico 1997), burned area assessment (Bruzzone and Prieto 2000), analysis of deforestation processes (Hame *et al.* 1998), identification of vegetation changes (Chavez and Mackinnon 1994), monitoring of urban growth (Merril and Jiajun 1998) and so on. Since all these applications usually require an analysis of a large area, development of automatic change-detection techniques is of high relevance in order to reduce the effort required by manual image analysis.

In the literature (Gopal and Woodcock 1996, Yuan *et al.* 2005, Canty 2006, Celik 2009), several supervised and unsupervised techniques for detecting changes in remote sensing images have been proposed. Supervised methods require the availability of 'ground truth' from which a training set, containing information about the spectral

*Corresponding author. Email: ash@isical.ac.in

signatures of the changes that occurred in the considered area between the two dates, is generated. The statistics of different classes can be more easily estimated, given the *a priori* information. Moreover, it is also possible to estimate the kind of changes occurred. In contrast, unsupervised approaches perform change detection without using any additional information, besides the raw images considered. The difficulty in collecting ground truth information regularly compelled researchers to develop unsupervised change-detection technique to support the analysis of temporal sequences of remote sensing images. The unsupervised change-detection problem can be viewed as a classification problem where, given the input image, a 'changed' class and an 'unchanged' class have to be distinguished.

Unsupervised change-detection techniques require three sequential steps (Singh 1989): (i) pre-processing, (ii) image comparison and (iii) image analysis. During pre-processing, two raw images are taken as input and are made compatible using operations like co-registration, radiometric and geometric corrections and noise reduction (Richards and Jia 2006). In the next step, two pre-processed images are compared pixel by pixel to generate a third image, called the difference image, where differences between the two acquisitions (images) are highlighted. There are several approaches to generate the difference image (Singh 1989). One of the most widely used approaches is the change vector analysis (CVA) technique, which differences out the two images (vectors) in order to produce a 'spectral change vector'. The grey value of the difference image is equal to the modulus of this change vector (Bovolo and Bruzzone 2007). Image analysis is performed on the difference image, in order to obtain a final change-detection map. Several image analysis techniques for unsupervised change detection already exist in the literature (Bruzzone and Prieto 2000, 2002, Kasetkasem and Varshney 2002, Bazi *et al.* 2005, Carincotte *et al.* 2006, Pajares 2006, Ghosh *et al.* 2007, 2009, Bovolo *et al.* 2008, Patra *et al.* 2008, Celik 2009). Although these techniques are robust to solve the change-detection problem, they are computationally expensive.

In the image analysis step, land-cover changes can also be detected using a decision threshold to the histogram of the difference image (Bruzzone and Prieto 2000, Melgani *et al.* 2002, Moser and Serpico 2006). For instance, when the CVA technique is used to generate the difference image, changed pixels can be identified on the right side of the histogram as they are associated with higher grey values and unchanged pixels can be identified on the left side of the histogram as they are associated with lower grey values. Therefore, a simple thresholding algorithm (Sezgin and Sankur 2004, Radke *et al.* 2005) may be used to distinguish between these two possibilities. Since in thresholding, only the evaluation of a criterion function is required and the algorithm is executed only once, it becomes fast. In addition, given the histogram, the computation time is independent of the size of the image. It depends only on the number of grey levels of the image. However, in this approach, the selection of the decision threshold is of major importance as the accuracy of the final change-detection map strongly depends on its choice. Since in many cases only a few changes occur in the study area between the two considered dates, the density function (histogram) of the pixel values in the difference image could be confused with the density function of the unchanged pixels. In this situation, conventional thresholding techniques will not be able to detect a suitable decision threshold. In this article to obtain a suitable threshold on the difference image, we have investigated several non-fuzzy and fuzzy global thresholding techniques that exist in the image processing literature.

2. Histogram thresholding

Let us consider two co-registered and radiometrically corrected γ-spectral band images X_1 and X_2, of size $p \times q$, acquired over the same area at different times T_1 and T_2, and let $D = \{l_{mn} | 1 \leq m \leq p, 1 \leq n \leq q, l_{mn} \in z, z = (0, 1, \ldots, L-1)\}$ be the difference image obtained by applying the CVA technique (Ghosh *et al.* 2009) to X_1 and X_2 with L possible grey levels. Then

$$l_{mn} = (\text{int}) \sqrt{\frac{1}{\gamma} \left(\sum_{\alpha=1}^{\gamma} \left(l_{mn}^{\alpha}(X_1) - l_{mn}^{\alpha}(X_2) \right)^2 \right)}.$$

Here $l_{mn}^{\alpha}(X_1)$ and $l_{mn}^{\alpha}(X_2)$ are the grey values of the pixels at the spatial position (m, n) in the αth band of images X_1 and X_2, respectively. Given a threshold value $t \in z$, the thresholded image (change-detection map) $D_t = \{l_{mn}(t)\}$ takes the following values:

$$l_{mn}(t) = \begin{cases} 0, & \text{if } l_{mn} < t \\ L-1, & \text{otherwise}. \end{cases} \tag{1}$$

Therefore, the purpose of thresholding is to classify the difference image into two groups, namely, ω_c and ω_u, corresponding to 'changed' and 'unchanged' classes. Let the number of pixels in the image with grey level i be f_i. Then the total number of pixels in the difference image is $\sum_{i=0}^{L-1} f_i (= p \times q)$. The probability of occurrence of grey level i (denoted as p_i) is

$$p_i = \frac{f_i}{p \times q}.$$

2.1 *Non-fuzzy thresholding*

In this section we will discuss a few popular classical thresholding techniques to be used to discriminate the changed and unchanged pixels of the difference image D.

2.1.1 Otsu's method. In this method (Otsu 1979), the optimal threshold t_1 is determined by analysing the behaviour of the variances of changed and unchanged classes obtained assuming different threshold values in the range 0 to $L-1$. Let $\sigma_W^2(t)$ and $\sigma_B^2(t)$ be the within-class variance and between-class variance, respectively, at threshold t and let σ^2 be the total variance. An optimal threshold t_1 can be determined by maximizing one of the following three criteria with respect to t:

$$\lambda = \frac{\sigma_B^2(t)}{\sigma_W^2(t)}, \quad \eta = \frac{\sigma_B^2(t)}{\sigma^2}, \quad \psi = \frac{\sigma^2}{\sigma_W^2(t)}. \tag{2}$$

As η is the simplest criterion among the three, in this study we have used it to obtain the optimal threshold t_1, which is obtained as follows:

$$t_1 = \text{Arg} \max_{t \in z} \{\eta\},$$

where $\sigma_B^2(t) = P_{\omega_u} P_{\omega_c} (\mu_{\omega_u} - \mu_{\omega_c})^2$ and $\sigma^2 = \Sigma_{i=0}^{L-1} (i-\mu)^2 p_i$, considering $\mu = \Sigma_{i=0}^{L-1} i p_i$, $\mu_{\omega_u} = \frac{\Sigma_{i=0}^{t} i p_i}{P_{\omega_u}}$, $\mu_{\omega_c} = \frac{\Sigma_{i=t+1}^{L-1} i p_i}{P_{\omega_c}}$, $P_{\omega_u} = \Sigma_{i=0}^{t} p_i$ and $P_{\omega_c} = 1 - P_{\omega_u}$.

2.1.2 Kapur's method. In this method (Kapur *et al.* 1985), the optimal threshold is determined based on the concept of entropy (Shannon 1948). Two probability distributions, one for ω_u and the other for ω_c, are derived from the original grey level distribution of the difference image D by assuming a threshold value t where,

$$\omega_u : \quad \frac{p_0}{P_{\omega_u}}, \frac{p_1}{P_{\omega_u}}, \ldots, \frac{p_t}{P_{\omega_u}}, \quad \text{and} \quad \omega_c : \quad \frac{p_{t+1}}{P_{\omega_c}}, \frac{p_{t+2}}{P_{\omega_c}}, \ldots, \frac{p_{L-1}}{P_{\omega_c}}.$$

The entropies of the unchanged (ω_u) and changed (ω_c) classes are then computed as

$$\begin{aligned} H_{\omega_u}(t) &= -\sum_{i=0}^{t} \frac{p_i}{P_{\omega_u}} \log_2 \left(\frac{p_i}{P_{\omega_u}} \right), \\ H_{\omega_c}(t) &= -\sum_{i=t+1}^{L-1} \frac{p_i}{P_{\omega_c}} \log_2 \left(\frac{p_i}{P_{\omega_c}} \right). \end{aligned} \tag{3}$$

The optimal threshold t_1 is selected by maximizing the total entropy $\{H_{\omega_u}(t) + H_{\omega_c}(t)\}$ using the following rule:

$$t_1 = \text{Arg} \max_{t \in z} \{H_{\omega_u}(t) + H_{\omega_c}(t)\}.$$

2.1.3 Kittler's method. In Kittler's method (Kittler and Illingworth 1986), the histogram is viewed as an estimate of the probability density function $p_D(i)$ of the mixture population comprising the grey levels of the changed and unchanged pixels. It is assumed that the probability density functions $p_{\omega_c}(.)$ and $p_{\omega_u}(.)$ of the changed and unchanged classes, respectively, are normally distributed with mean μ_{ω_c} and μ_{ω_u}, and standard deviation σ_{ω_c} and σ_{ω_u}. Let P_{ω_c} and P_{ω_u} be the *a priori* probability of ω_c and ω_u, respectively. The probability density function $p_D(.)$ of the mixture model is written as

$$p_D(i) = P_{\omega_u}\, p_{\omega_u}(i) + P_{\omega_c}\, p_{\omega_c}(i), \tag{4}$$

where

$$p_{\omega_u}(i) = \frac{1}{\sqrt{2\pi}\sigma_{\omega_u}} \exp\left[-\frac{(i-\mu_{\omega_u})^2}{2\sigma_{\omega_u}^2} \right] \text{and} \, p_{\omega_c}(i) = \frac{1}{\sqrt{2\pi}\sigma_{\omega_c}} \exp\left[-\frac{(i-\mu_{\omega_c})^2}{2\sigma_{\omega_c}^2} \right].$$

According to Bayes' rule the minimum error threshold t_1 is obtained by solving the following quadratic equation:

$$\frac{(i-\mu_{\omega_u})^2}{2\sigma_{\omega_u}^2} + \log \sigma_{\omega_u}^2 - 2 \log P_{\omega_u} = \frac{(i-\mu_{\omega_c})^2}{2\sigma_{\omega_c}^2} + \log \sigma_{\omega_c}^2 - 2 \log P_{\omega_c}. \tag{5}$$

To find out the minimum error threshold t_1, instead of solving the above quadratic equation, Kittler and Illingworth (1986) defined a criterion function $J(t)$ for threshold t as follows:

$$J(t) = 1 + 2(P_{\omega_u} \log \sigma_{\omega_u} + P_{\omega_c} \log \sigma_{\omega_c}) - 2(P_{\omega_u} \log P_{\omega_u} + P_{\omega_c} \log P_{\omega_c}), \tag{6}$$

where

$$\sigma^2_{\omega_u} = \frac{\left[\Sigma_{i=0}^{t}(i - \mu_{\omega_u})^2 p_i\right]}{P_{\omega_u}} \quad \text{and} \quad \sigma^2_{\omega_c} = \frac{\left[\Sigma_{i=t+1}^{L-1}(i - \mu_{\omega_c})^2 p_i\right]}{P_{\omega_c}}.$$

The optimal threshold t_1 is obtained by minimizing $J(t)$, that is,

$$t_1 = \text{Arg} \min_{t \in z}\{J(t)\}.$$

2.2 *Fuzzy thresholding*

Fuzzy set theory is a generalization of classical set theory. It has the flexibility of capturing various aspects of incompleteness or imperfection in the information of a situation. The flexibility of fuzzy set theory is associated with the concept of its membership function. The higher the value of membership, the lesser will be the amount to which the concept represented by a set needs to be stretched to fit an object. Since the regions in an image are not always crisply defined (due to both greyness ambiguity and geometrical ambiguity), the use of hard decisions for image classification may not work well. Thus, it is natural to consider fuzzy sets for these kinds of problems (Pal and Ghosh 1992a).

Let $\mu_D(l_{mn})$ denote the membership value representing the degree of possessing a certain property by the (m,n) pixel in D. In the notation of fuzzy sets (Pal and Dutta Majumder 1986), the image set D can be written as

$$D = \{(l_{mn}), (\mu_D(l_{mn}))\},$$

where $0 < \mu_D(l_{mn}) \leq 1$. The membership value of a pixel in D can be defined by considering its degree of belonging to the changed and unchanged classes. In the following sections, we will discuss some fuzzy thresholding techniques that exist in the image processing literature.

2.2.1 Fuzzy ambiguity minimization methods. Most of the thresholding techniques are based on the measure of fuzzy greyness ambiguity (DeLuca and Termini 1972, Pal and Ghosh 1992b) and fuzzy geometrical ambiguity (Rosenfeld 1984, Pal and Ghosh 1992a). The optimal threshold is selected by minimizing the fuzzy ambiguity. All the thresholding techniques, based on the minimization of fuzzy ambiguity, follow the same procedure. Here we will discuss only fuzzy entropy and fuzzy correlation-based ambiguity measures (the latter is to be maximized) to be used to select the optimal threshold. Let us construct a fuzzy subset *bright* image characterized by a membership function $\mu_D(.)$ using the standard $S(i; a, b, c)$ function of Zadeh (1965). It is defined as

$$\mu_D(i) = \begin{cases} 0 & \text{if } i \leq a \\ 2\{(i-a)/(c-a)\}^2 & \text{if } a \leq i \leq b \\ 1 - 2\{(i-c)/(c-a)\}^2 & \text{if } b \leq i \leq c, \\ 1 & \text{if } c \leq i \end{cases} \tag{7}$$

where $\mu_D(i)$ ($i \in z$) is a function of grey level only and represents the degree of belonging of the level i to the fuzzy *bright* image; $b = (a + c)/2$ is the crossover point (for which the membership value is 0.5) of the membership function μ_D. The fuzzy entropy at threshold $t = b$ of an image D is (DeLuca and Termini 1972)

$$H(t) = \frac{\sum_{i=0}^{L-1}[-\mu_D(i)\ln(\mu_D(i)) - (1-\mu_D(i))\ln(1-\mu_D(i))]f_i}{(p \times q)\ln 2}. \tag{8}$$

Let $\mu_{\bar{D}}(.)$ be the nearest two tone version of $\mu_D(.)$ such that

$$\mu_{\bar{D}}(i) = \begin{cases} 0 & \text{if } 0 \le \mu_D(i) \le 0.5 \\ 1 & \text{otherwise.} \end{cases} \tag{9}$$

The fuzzy correlation between a fuzzy representation of an image and its nearest two tone version for a threshold $t = b$ is expressed as (Pal and Ghosh 1992b)

$$\mathrm{Cor}(t) = 1 - \frac{4}{C_1 + C_2}\left(\sum_{i=0}^{t}\{[\mu_D(i)]^2 f_i\} + \sum_{i=t+1}^{L-1}\{[1-\mu_D(i)]^2 f_i\}\right), \tag{10}$$

with $C_1 = \sum_{i=0}^{L-1}[2\mu_D(i) - 1]^2 f_i$ and $C_2 = \sum_{i=0}^{L-1}[2\mu_{\bar{D}}(i) - 1]^2 f_i = \sum_{i=0}^{L-1} f_i = p \times q$.

Here we write the whole process in the form of an algorithm.

Algorithm for threshold selection: Given an image D with minimum and maximum grey value $L_{\min}$ and $L_{\max}$, respectively, the algorithm to determine the optimal threshold t_1 is given below:

Step 1: Construct the membership plane using the standard $S(i; a, b, c)$ function as $\mu_D(i) = S(i; a, t, c)$ with crossover point t, and bandwidth $\Delta t = t - a = c - t$.

Step 2: Vary t between $L_{\min}$ and $L_{\max}$. Compute the entropy $H(t)$ and correlation $\mathrm{Cor}(t)$ for different values of t using equations (8) and (10), respectively.

Step 3: Select the optimal threshold t_1 for which $H(t_1)$ has a global minimum or $\mathrm{Cor}(t_1)$ has a global maximum, that is,

$$t_1 = \mathrm{Arg}\ \min_{(t=b)\in z}\{H(t)\} \quad or \quad t_1 = \mathrm{Arg}\ \max_{(t=b)\in z}\{\mathrm{Cor}(t)\}.$$

The above threshold selection techniques, based on entropy minimization and correlation maximization, will be referred to as DeLuca-Entropy (DeLuca and Termini 1972) and Pal-Correlation (Pal and Ghosh 1992b) technique, respectively, in the subsequent sections.

2.2.2 Huang's method. In this method (Huang and Wang 1995), assuming a certain threshold value t, the average grey levels of the changed pixels μ_{ω_c} and the unchanged pixels μ_{ω_u} are computed. These average grey levels, μ_{ω_c} and μ_{ω_u}, can be considered as the target values of the changed and unchanged regions for the given threshold t. The membership function for a pixel with grey value i in D is then defined as

$$\mu_D(i) = \begin{cases} \frac{1}{1+|i-\mu_{\omega_u}|/C} & \text{if } i \le t \\ \frac{1}{1+|i-\mu_{\omega_c}|/C} & \text{if } i > t, \end{cases} \tag{11}$$

where C is a constant and set in a way so that $0.5 \leq \mu_D(i) \leq 1$. To measure the fuzziness of the fuzzy set, Huang and Wang introduced two commonly used measures: one is entropy measure (Pal and Dutta Majumder 1986) and the other is Yager's measure (Yager 1979).

Entropy measure: For threshold t, the entropy $H(t)$ of an image D is computed by equation (8) using the membership function defined in equation (11).

Yager's measure: Yager's measure is based on the distance between a fuzzy image subset D and its complement $\acute{D}$ as follows:

$$Y_\rho(D, \acute{D}) = \left[\sum_{i=0}^{L-1} |\mu_D(i) - \mu_{\acute{D}}(i)|^\rho f_i\right]^{1/\rho}, \quad \rho = 1, 2, 3, \ldots, \tag{12}$$

where $\mu_{\acute{D}}(i) = 1 - \mu_D(i)$. Assuming threshold t, the measure of fuzziness of D can be computed as

$$\xi(t) = 1 - \frac{Y_\rho(D, D')}{(p \times q)^{1/\rho}}. \tag{13}$$

When $\mu_D(i) = 0.5$, $\forall i$, both the measures defined in equations (8) and (13) will have maximum value of fuzziness. On the other hand, when $\mu_D(i) = 1$, $\forall i$, both the measures will have minimum value of fuzziness. Considering different thresholds t, the fuzziness of the image D is measured using either entropy or Yager's measure. The optimal threshold t_1 is selected where the measure of fuzziness is minimal, that is,

$$t_1 = \text{Arg} \min_{t \in z}\{H(t)\} \quad or \quad t_1 = \text{Arg} \min_{t \in z}\{\xi(t)\}.$$

The above threshold selection techniques based on the entropy measure and Yager's measure will be referred to as the Huang-Entropy and Huang-Yager techniques, respectively, in this work.

2.2.3 Liu's method. Using fuzzy entropy, several threshold selection algorithms have been proposed in the image processing literature (Huang and Wang 1995, Cheng *et al.* 1998, 1999, 2000, Tao *et al.* 2003, Liu *et al.* 2006). Liu *et al.* (2006) selected the optimal threshold t_1 based on a fuzzy entropy measure which considers both inter-class distinctness and intra-class variation. As defined by Huang and Wang (1995), the fuzzy membership value for a pixel with grey value i in D is obtained using equation (11). The fuzzy entropies of unchanged (ω_u) and changed (ω_c) classes, denoted as $H_{\omega_u}(t)$ and $H_{\omega_c}(t)$, respectively, are then computed as

$$\begin{aligned} H_{\omega_u}(t) &= -\sum_{i=0}^{t} \frac{p_i}{\mu_D(i)P_{\omega_u}} \log \frac{p_i}{\mu_D(i)P_{\omega_u}}, \\ H_{\omega_c}(t) &= -\sum_{i=t+1}^{L-1} \frac{p_i}{\mu_D(i)P_{\omega_c}} \log \frac{p_i}{\mu_D(i)P_{\omega_c}}, \end{aligned} \tag{14}$$

where $P_{\omega_u} = \sum_{i=0}^{t} \frac{p_i}{\mu_D(i)}$ and $P_{\omega_c} = \sum_{i=t+1}^{L-1} \frac{p_i}{\mu_D(i)}$.

Equation (14) defines the entropy of distribution of the ratio of the grey-scale histogram and fuzzy membership of unchanged and changed pixels for threshold t. The optimal threshold t_1 is selected by maximizing $\{H_{\omega_u}(t) + H_{\omega_c}(t)\}$ over t, that is,

$$t_1 = \text{Arg} \max_{t \in z} \{H_{\omega_u}(t) + H_{\omega_c}(t)\}.$$

3. Description of the data sets

In order to carry out the experimental analysis aimed at assessing the effectiveness of different thresholding approaches, we considered three different multitemporal data sets corresponding to geographical areas of Mexico, the Island of Sardinia, Italy, and the Peloponnesian Peninsula, Greece. A detailed description of each of the data sets is given below.

3.1 *Data set related to the Mexico area*

The first data set used in the experiment is made up of two multispectral images acquired by the Landsat Enhanced Thematic Mapper Plus (ETM+) sensor of the Landsat-7 satellite in an area of Mexico on 18 April 2000 and 20 May 2002. From the entire available Landsat scene, a section of 512 × 512 pixels has been selected as test site. Between the two aforementioned acquisition dates, a fire destroyed a large portion of the vegetation in the region. Figure 1(*a*) and 1(*b*) shows channel 4 of the 2000 and 2002 images, respectively. In order to be able to make a quantitative evaluation of the effectiveness of the proposed approach, a reference map was manually defined (see figure 1(*d*)) according to a detailed visual analysis of both the available multitemporal images and the difference image (shown in figure 1(*c*)). Different colour composites of these images were used to highlight all the portions of the changed area in the best possible way. This procedure resulted in a reference map containing 25 599 changed and 236 545 unchanged pixels.

Analysis of the behaviour of the histograms of multitemporal images did not reveal any significant difference due to light and atmospheric conditions at the acquisition dates. Therefore, no radiometric correction algorithm was applied. The 2002 image was registered on the 2000 image using 12 ground control points. The procedure led to a residual average misregistration error on ground control points of about 0.3 pixels.

3.2 *Data set related to the Island of Sardinia, Italy*

The second data set used in the experiment is composed of two multispectral images acquired by the Landsat Thematic Mapper (TM) sensor of the Landsat-5 satellite in September 1995 and July 1996. The test site is a section of 412 × 300 pixels of a scene including Lake Mulargia on the Island of Sardinia, Italy. Between the two aforementioned acquisition dates, the water level in the lake increased (see the lower central part of the image). Figure 2(*a*) and 2(*b*) shows channel 4 of the 1995 and 1996 images. As done for the Mexico data set, in this case also a reference map was manually defined (see figure 2(*d*)) according to a detailed visual analysis of both the available multitemporal images and the difference image (see figure 2(*c*)). In the end, 7480 changed and 116 120 unchanged pixels were identified. As the histograms did not show any significant difference, no radiometric correction algorithm was applied to the multitemporal images. The images were co-registered with 12 ground control points resulting in an average residual misregistration error of about 0.2 pixels on the ground control points.

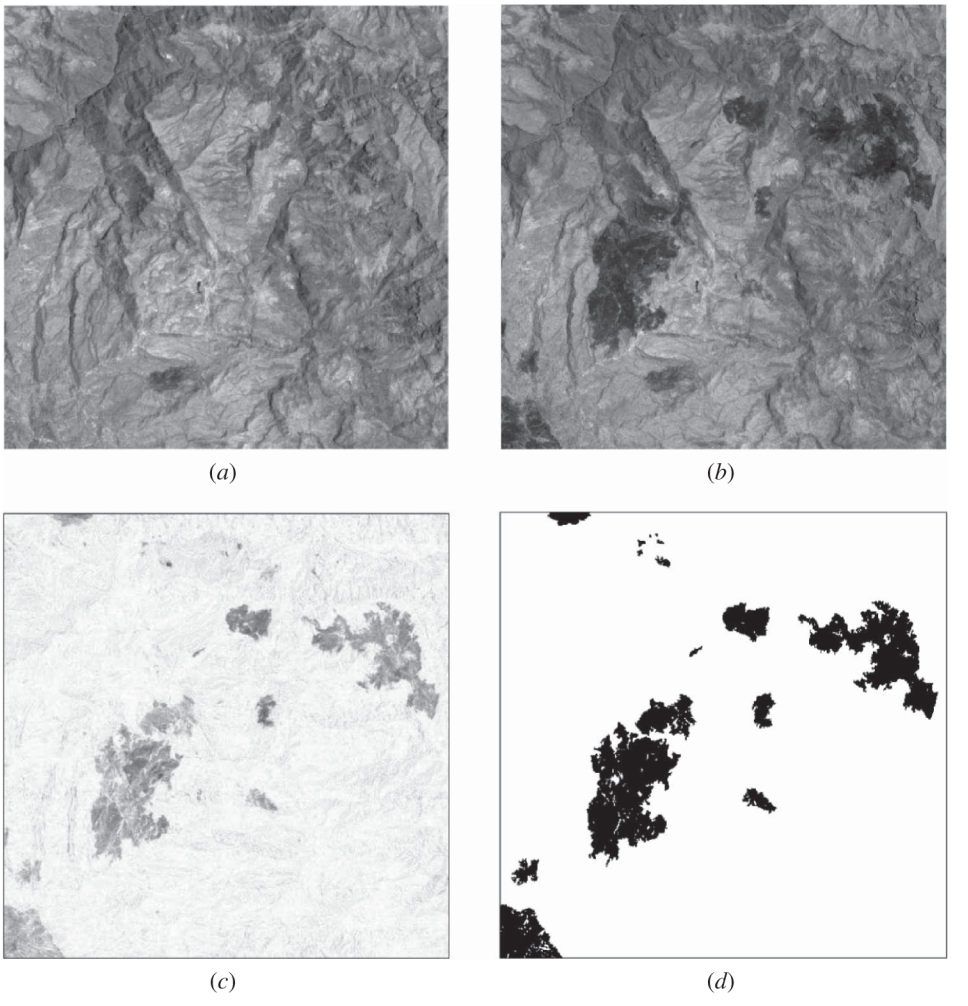

Figure 1. Image of the Mexico area. (*a*) Band 4 of the Landsat ETM+ image acquired in April 2000, (*b*) band 4 of the Landsat ETM+ image acquired in May 2002, (*c*) corresponding difference image generated by the CVA technique and (*d*) reference map of the changed area.

3.3 *Data set related to the Peloponnesian Peninsula, Greece*

The third data set used in the experiment is composed of two images acquired of the same area by a passive multispectral scanner installed on a satellite, that is, the Wide Field Sensor (WiFS) mounted on board the IRS-P3 satellite. The area shown in the two images is a section (492 × 492 pixels) of a scene acquired in the southern part of the Peloponnesian Peninsula, Greece, in April 1998 and September 1998. As an example, figure 3(*a*) and 3(*b*) shows channel 2 (i.e. near-infrared spectral channels) of both the images. As is readily apparent, various wildfires destroyed a significant portion of the vegetation in the aforesaid area between the two dates. Like the previously mentioned data sets, a reference map was manually defined (see figure 3(*d*)) to assess change-detection errors. This reference map contains 5197 changed and

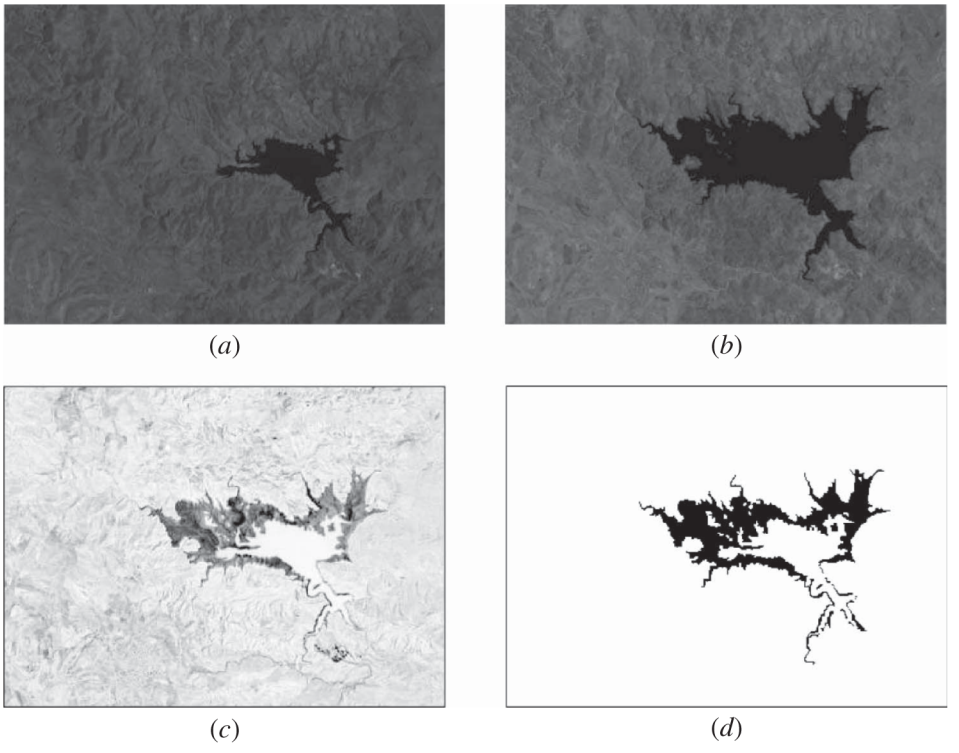

Figure 2. Image of Sardinia Island, Italy. (*a*) Band 4 of the Landsat TM image acquired in September 1995; (*b*) band 4 of the Landsat TM image acquired in July 1996; (*c*) corresponding difference image generated by the CVA technique using bands 1, 2, 4 and 5; and (*d*) reference map of the changed area.

236 867 unchanged pixels. The images were registered using the multispectral image acquired in April as a reference image. The analysis of the histograms of the April and September images did not reveal any significant difference in the light conditions at the two dates.

4. Experimental methods

In this work, an investigation is carried out to check the suitability of various histogram thresholding techniques, applied on the difference image, for generating change-detection maps. The change-detection results provided by these techniques are compared with those produced by the Manual Trial-and-Error Thresholding (MTET) technique. The MTET technique generates a minimum error change-detection map under the hypothesis of spatial independence among the pixels by finding a minimum error decision threshold for the difference image. The minimum error decision threshold is obtained by computing the change-detection error (with the help of the reference map) for all possible values of the decision threshold. Comparisons are carried out in terms of both overall error (OE), number of false alarms (i.e. unchanged pixels identified as changed ones, denoted as FA) and number of missed alarms (i.e. changed pixels categorized as unchanged ones, denoted as MA).

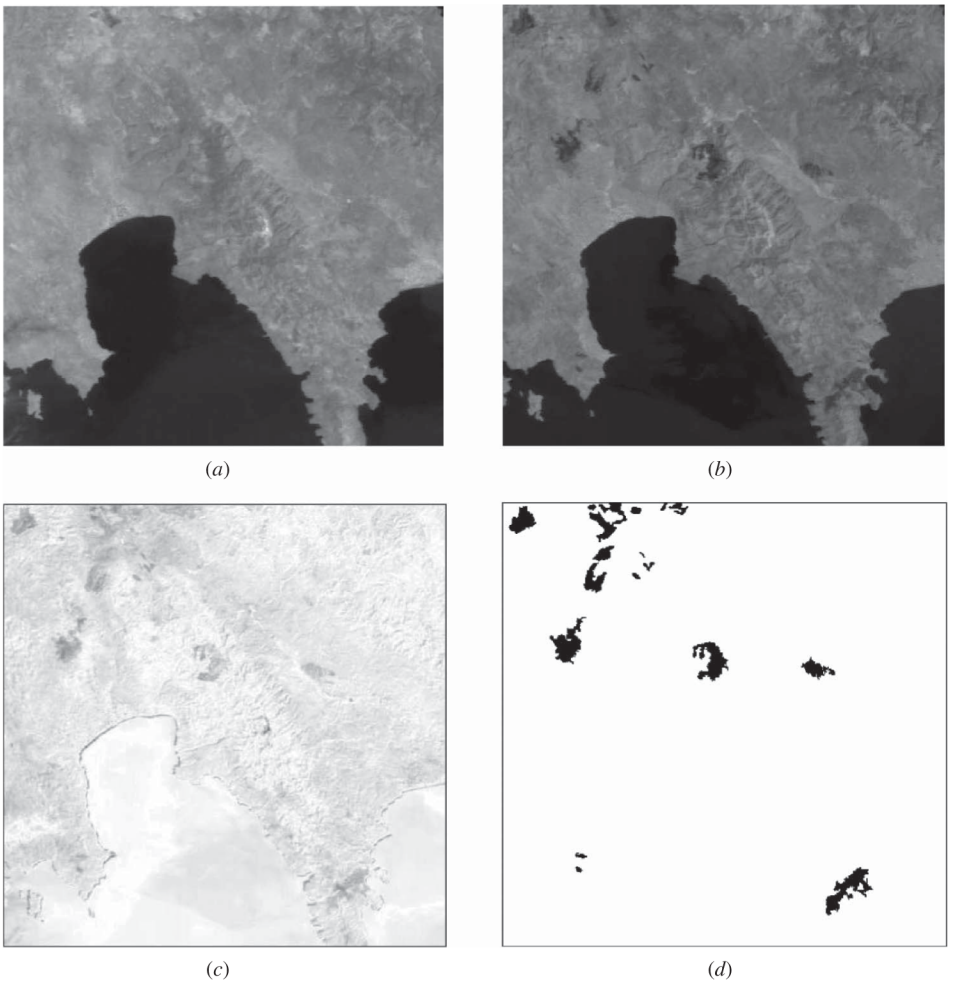

Figure 3. Images of the Peloponnesian Peninsula, Greece. (*a*) NIR band of the IRS-PE WiFS image acquired in April 1998, (*b*) NIR band of the IRS-PE WiFS image acquired in September 1998, (*c*) corresponding difference image generated by the CVA technique using the NIR band and (*d*) reference map of the changed area.

4.1 *Analysis of results*

Table 1 shows the change-detection results obtained by different thresholding techniques. For the Mexico data set, it is found that, except for Kittler's method, all methods detected thresholds which are close to the optimal threshold ($t_1 = 39$) derived by the MTET technique. For visual analysis, figure 4 depicts the change-detection maps produced by these techniques. It is apparent that the techniques which select higher threshold values produce higher MA and lower FA, whereas the techniques which select lower threshold values produce lower MA and higher FA.

For the Sardinia data set, by analysing the results shown in table 1, it is seen that Kittler's and Huang's (Huang-Entropy and Huang-Yager) methods fail to detect

Table 1. Detected thresholds (t_1) and the corresponding change-detection results obtained by applying different thresholding techniques.

	Mexico data		Sardinia Island data		Peloponnesian Peninsula data	
Methods used	t_1	OE (MA+FA)	t_1	OE (MA+FA)	t_1	OE (MA+FA)
MTET	39	4591 (2404+2187)	95	1890 (1015+875)	64	3553 (2424+1129)
Otsu's method	45	5111 (3860+1251)	73	6122 (199+5923)	26	65518 (65+65453)
Kapur's method	37	4697 (1981+2716)	84	3051 (458+2593)	55	4845 (1395+3450)
Kittler's method	24	15131 (0+15131)	62	12824 (77+12747)	24	75873 (47+75826)
DeLuca-Entropy	38	4625 (2187+2438)	88	2343 (645+1698)	64	3553 (2424+1129)
Pal-Correlation	36	4811 (1743+3068)	88	2343 (645+1698)	60	3724 (1891+1833)
Huang-Entropy	31	6445 (760+5685)	46	30643 (19+30624)	19	109602 (19+109583)
Huang-Yager	42	4776 (3131+1645)	49	25825 (26+25799)	19	109602 (19+109583)
Liu's method	39	4591 (2404+2187)	85	2645 (545+2100)	55	4845 (1395+3450)

the proper threshold and also Otsu's method detected a threshold which is far away from the optimal threshold ($t_1 = 95$) as detected by the MTET technique. All other methods, for example, Kapur's, DeLuca-Entropy, Pal-Correlation and Liu's methods, detected thresholds which are close to the optimal one. For visual illustration, the change-detection maps produced by all these techniques are shown in figure 5.

By analysing the results shown in table 1 for the Peloponnesian Peninsula data set, it is noticed that Kapur's, DeLuca-Entropy, Pal-Correlation and Liu's methods are able to detect the proper thresholds which are close to the optimal threshold ($t_1 = 64$) obtained by applying the MTET technique. The other methods failed to find a suitable threshold. Figure 6 shows the change-detection maps produced by different techniques. Visual analysis also conform the above findings.

It should be noted that Otsu's method detects a threshold by maximizing the between-class variance criterion. This criterion may fail to select the proper threshold when the size of the changed and unchanged regions are significantly different irrespective of their intensity contrast (Qiao *et al.* 2007). For the Sardinia and Peloponnesian Peninsula data sets, since the sizes of the unchanged regions are much larger than the changed regions (see figures 2(*d*) and 3(*d*)), Otsu's method detected thresholds which are far away from the optimal one found by the MTET technique.

In Kapur's method the optimal threshold is detected by maximizing the entropy of the changed and unchanged classes. It tries to modify the histogram of the difference image so as to have a more or less equal distribution for changed and unchanged

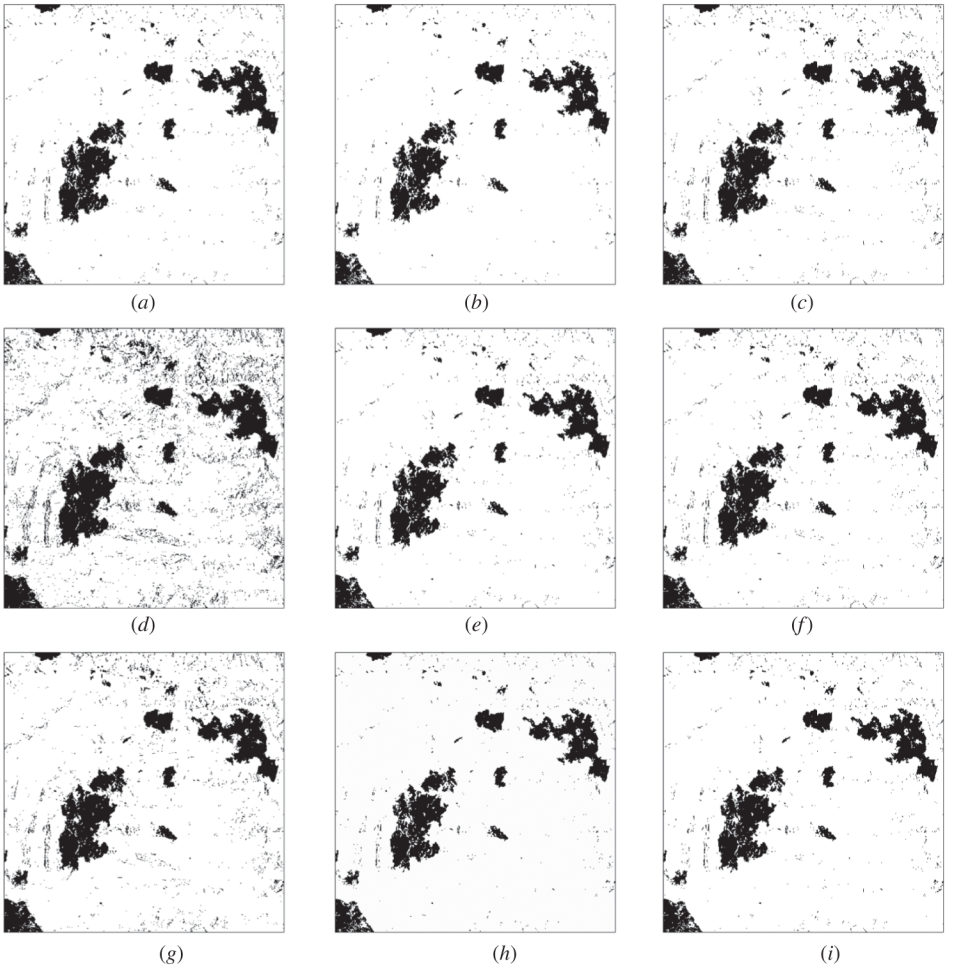

Figure 4. Change-detection maps (black and white represent the changed and the unchanged areas, respectively) obtained for the Mexico data set using (*a*) MTET, (*b*) Otsu's method, (*c*) Kapur's method, (*d*) Kittler's method, (*e*) DeLuca-Entropy, (*f*) Pal-Correlation, (*g*) Huang-Entropy, (*h*) Huang-Yager and (*i*) Liu's method.

classes. As the method uses the *a priori* probability of both the classes to modify the distribution of the histogram, unlike Otsu's method, it selects a threshold irrespective of the sizes of the changed and unchanged regions. Also, unlike Kittler's method it is independent of the distributions of the two classes. Kapur's method is considered to be one of the best approaches to thresholding (Radke *et al.* 2005). In this investigation, for all the data sets, the results obtained by this method also confirm the validity of the above findings.

Kittler's method defines a criterion based on the assumption that the histograms of the changed and unchanged pixels are normally distributed and a threshold is selected by minimizing this criterion. The smaller the overlap between the density functions of the changed and unchanged pixels, the lower is the criterion value. Figure 7 shows the histograms of the difference image of the Mexico, Sardinia and Peloponnesian

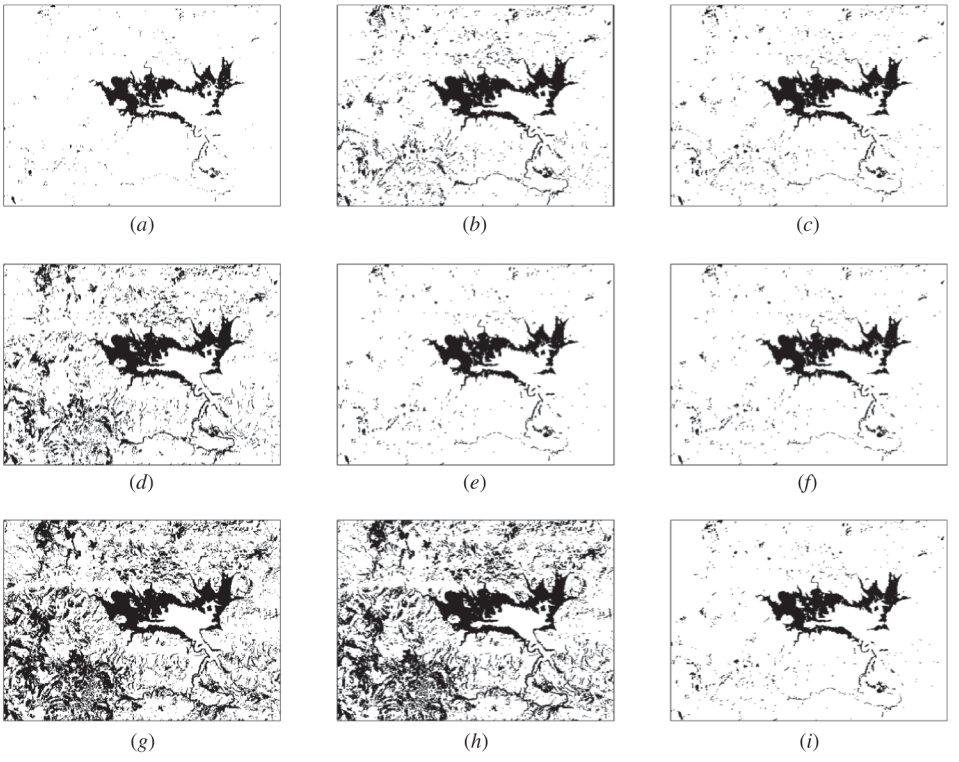

Figure 5. Change-detection maps (black and white represent the changed and the unchanged areas, respectively) obtained for the Sardinia Island data set using (*a*) MTET, (*b*) Otsu's method, (*c*) Kapur's method, (*d*) Kittler's method, (*e*) DeLuca-Entropy, (*f*) Pal-Correlation, (*g*) Huang-Entropy, (*h*) Huang-Yager and (*i*) Liu's method.

Peninsula data sets. From these histograms we can say that the density function of the pixel values in the difference image can be confused with the density function of the unchanged pixels. As a result, the overlap between the density functions of the changed and unchanged pixels becomes a minimum when the threshold is far left of the optimal threshold. The results shown in table 1 confirm the validity of these findings.

In fuzzy ambiguity minimization techniques, users have to specify the width of the window w ($w = 2\Delta t$), which is shifted over the dynamic range of the fuzzy region of the histogram. Depending on the size of the window, different global thresholds may be detected. In this experiment, the value of w was chosen by the trial-and-error method. From the results it is seen that, for all the considered data sets, the fuzzy ambiguity minimization techniques detected the thresholds which are close to the optimal threshold (obtained by MTET).

Thresholds detected by Huang's method (both Huang-Entropy and Huang-Yager) depend on the statistical mean of the assumed changed and unchanged classes (Melgani *et al.* 2002). In this experiment, this method produces good thresholds for the Mexico data set, but fails to produce acceptable thresholds for the Sardinia and Peloponnesian Peninsula data sets. This may be because only information (class mean) on which the technique relies may not be a proper representation of the classes to detect an appropriate threshold.

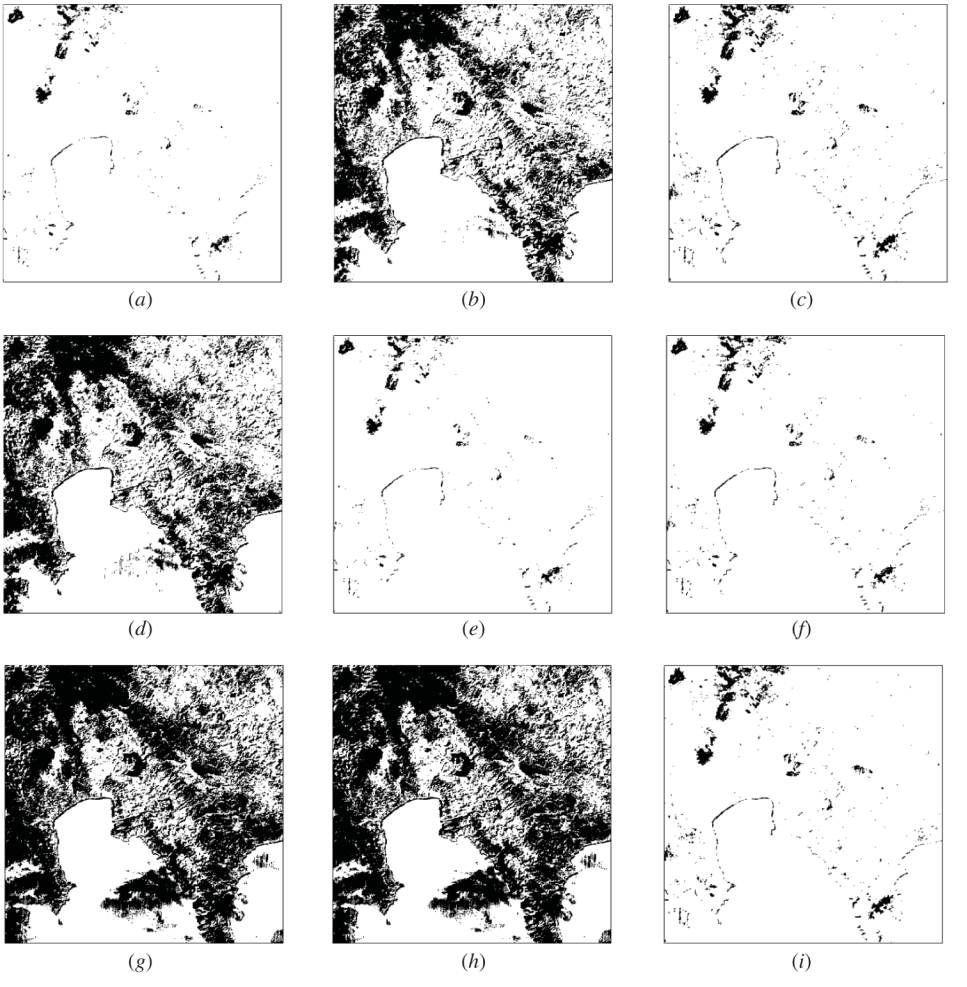

Figure 6. Change-detection maps (black and white represent the changed and the unchanged areas, respectively) obtained for the Peloponnesian Peninsula data set using (*a*) MTET, (*b*) Otsu's method, (*c*) Kapur's method, (*d*) Kittler's method, (*e*) DeLuca-Entropy, (*f*) Pal-Correlation, (*g*) Huang-Entropy, (*h*) Huang-Yager and (*i*) Liu's method.

Liu's method produced good results for all three data sets used in this experiment. Unlike Huang's method, Liu's method considers not only inter-class distinctness, but also intra-class variation which may help select better thresholds. Basically, the entropy defined by Liu contains Kapur's entropy (Kapur *et al.* 1985) in itself and introduces a fuzzy concept to manage the natural fuzziness of images.

In this experiment, we have used three multitemporal remote sensing data sets for two different applications. The Mexico and Peloponnesian Peninsula data sets are used to assess the burned regions and the Sardinia data set is used to assess the flood-affected regions. From these applications, we found that the fuzzy ambiguity minimization methods (DeLuca-Entropy and Pal-Correlation), Liu's method and Kapur's method are the most effective thresholding techniques. All these methods

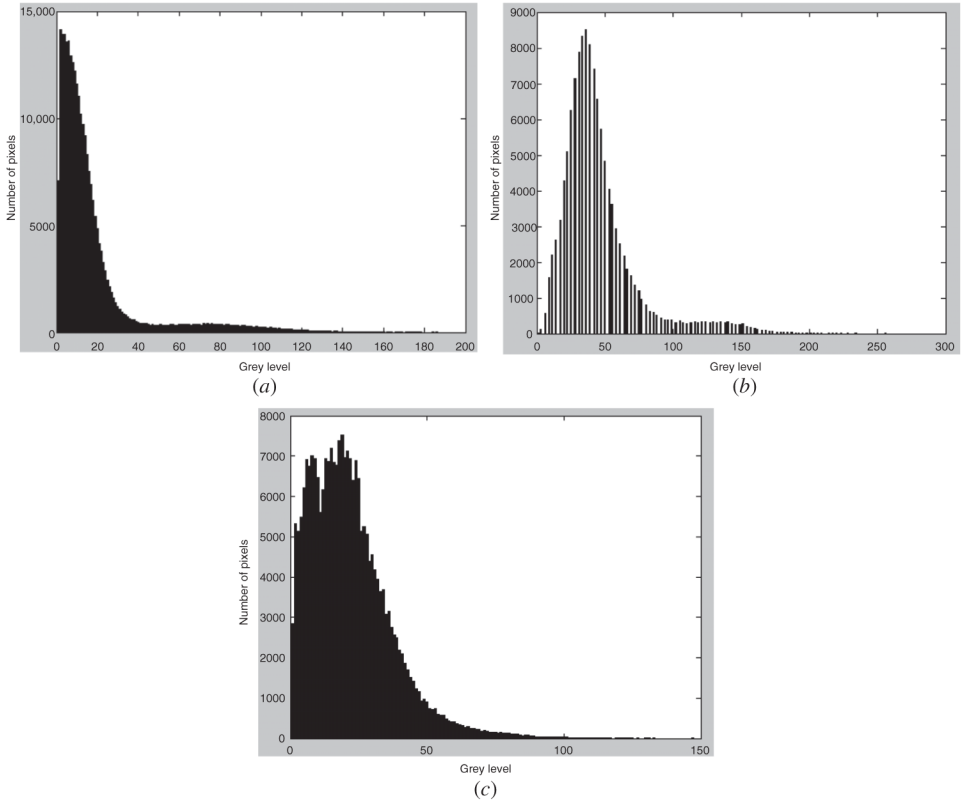

Figure 7. Histograms of the difference image generated by using the multitemporal images of (*a*) the Mexico area, (*b*) Sardinia Island, Italy and (*c*) the Peloponnesian Peninsula, Greece.

provided fewer MA compared to the MTET method which is sometimes important for this kind of application.

5. Conclusions

Histogram thresholding is one of the cheapest and fastest techniques for unsupervised image classification. In the present work, several global non-fuzzy and fuzzy thresholding techniques have been used and compared for detecting changes of multitemporal remote sensing images. All the described techniques are used to detect thresholds from the histogram of the difference image that represents the modulus of the spectral change vectors associated with each pixel in the study area.

Considering the present investigation, among the various thresholding techniques, fuzzy ambiguity minimization techniques (DeLuca-Entropy and Pal-Correlation) produced the best results (compared to other non-fuzzy and fuzzy techniques), but they need an appropriate window size as an input parameter from the users. On the other hand, Liu's fuzzy entropy-based technique also provided better performance, followed by Kapur's non-fuzzy entropy-based technique without using any user-defined parameters. All other algorithms are found to show moderate performance. In this regard, we plan to do some more investigations for multidimensional histogram thresholding which take local information into account.

As a final remark, the histogram thresholding-based change-detection methods are simple and suitable for applications like management of natural resources (e.g. forests, sea), damage mapping (e.g. burned areas, floods areas, earthquake) and so on. However, their suitability for land-use and land-cover change detection is limited.

Acknowledgements

The authors thank the anonymous referees for their constructive criticism and valuable suggestions. The authors thank the Department of Science and Technology, Government of India and University of Trento, Italy, the sponsors of the ITPAR program and Prof. L. Bruzzone, the Italian collaborator of this project, for providing the data.

References

Bazi, Y., Bruzzone, L. and Melgani, F., 2005, An unsupervised approach based on the generalized Gaussian model to automatic change detection in multitemporal SAR images. *IEEE Transactions on Geoscience and Remote Sensing*, **43**, pp. 874–887.

Bovolo, F. and Bruzzone, L., 2007, A theoretical framework for unsupervised change detection based on change vector analysis in the polar domain. *IEEE Transactions on Geoscience and Remote Sensing*, **45**, pp. 218–236.

Bovolo, F., Bruzzone, L. and Marconcini, M., 2008, A novel approach to unsupervised change detection based on a semisupervised SVM and a similarity measure. *IEEE Transactions on Geoscience and Remote Sensing*, **46**, pp. 2070–2082.

Bruzzone, L. and Prieto, D.F., 2000, Automatic analysis of the difference image for unsupervised change detection. *IEEE Transactions on Geoscience and Remote Sensing*, **38**, pp. 1171–1182.

Bruzzone, L. and Prieto, D.F., 2002, An adaptive semiparametric and context-based approach to unsupervised change detection in multitemporal remote-sensing images. *IEEE Transactions on Image Processing*, **11**, pp. 452–466.

Bruzzone, L. and Serpico, S.B., 1997, An iterative technique for the detection of land-cover transitions in multitemporal remote-sensing images. *IEEE Transactions on Geoscience and Remote Sensing*, **35**, pp. 858–867.

Canty, M.J., 2006, *Image Analysis, Classification and Change Detection in Remote Sensing* (Boca Raton, FL: Taylor & Francis, CRC Press).

Carincotte, C., Derrode, S. and Bourennane, S., 2006, Unsupervised change detection on SAR images using fuzzy hidden Markov chains. *IEEE Transactions on Geoscience and Remote Sensing*, **44**, pp. 432–441.

Celik, T., 2009, Unsupervised change detection in satellite images using principal component analysis and *k*-means clustering. *IEEE Transactions on Geoscience and Remote Sensing Letters*, **6**, pp. 772–776.

Chavez Jr., P.S. and MacKinnon, D.J., 1994, Automatic detection of vegetation changes in the southwestern United States using remotely sensed images. *Photogrammetric Engineering and Remote Sensing*, **60**, pp. 1285–1294.

Cheng, H.D., Chen, J.R. and Li, J., 1998, Threshold selection based on fuzzy c-partition entropy approach. *Pattern Recognition*, **31**, pp. 857–870.

Cheng, H.D., Chen, Y.H. and Jiang, X.H., 2000, Thresholding using two dimensional histogram and fuzzy entropy principle. *IEEE Transactions on Image Processing*, **9**, pp. 732–735.

Cheng, H.D., Chen, Y.H. and Sun, Y., 1999, A novel fuzzy entropy approach to image enhancement and thresholding. *Signal Processing*, **75**, pp. 277–301.

Cihlar, J., Pultz, T.J. and Gray, A.L., 1992, Change detection with synthetic aperture radar. *International Journal of Remote Sensing*, **13**, pp. 401–414.

DeLuca, A. and Termini, S., 1972, A definition of a non probabilistic entropy in the setting of fuzzy sets theory. *Information and Control*, **20**, pp. 301–312.

Ghosh, S., Bruzzone, L., Patra, S., Bovolo, F. and Ghosh, A., 2007, A context-sensitive technique for unsupervised change detection based on Hopfield-type neural networks. *IEEE Transactions on Geoscience and Remote Sensing*, **45**, pp. 778–789.

Ghosh, S., Patra, S. and Ghosh, A., 2009, An unsupervised context-sensitive change detection technique based on modified self-organizing feature map neural network. *International Journal of Approximate Reasoning*, **50**, pp. 37–50.

Gopal, S. and Woodcock, C., 1996, Remote sensing of forest change using artificial neural networks. *IEEE Transactions on Geoscience and Remote Sensing*, **34**, pp. 398–404.

Hame, T., Heiler, I. and Miguel-Ayanz, J.S., 1998, An unsupervised change detection and recognition system for forestry. *International Journal of Remote Sensing*, **19**, pp. 1079–1099.

Huang, L.K. and Wang, M.J.J., 1995, Image thresholding by minimizing the measures of fuzziness. *Pattern Recognition*, **28**, pp. 41–51.

Kapur, J.N., Sahoo, P.K. and Wong, A.K.C., 1985, A new method for gray-level picture thresholding using the entropy of the histogram. *Computer Vision, Graphics, and Image Processing*, **29**, pp. 273–285.

Kasetkasem, T. and Varshney, P.K., 2002, An image change detection algorithm based on Markov random field models. *IEEE Transactions on Geoscience and Remote Sensing*, **40**, pp. 1815–1823.

Kittler, J. and Illingworth, J., 1986, Minimum error thresholding. *Pattern Recognition*, **19**, pp. 41–47.

Liu, D., Jiang, Z. and Feng, H., 2006, A novel fuzzy classification entropy approach to image thresholding. *Pattern Recognition Letters*, **27**, pp. 1968–1975.

Melgani, F., Moser, G. and Serpico, S.B., 2002, Unsupervised change-detection methods for remote-sensing data. *Optical Engineering*, **41**, pp. 3288–3297.

Merril, K.R. and Jiajun, L., 1998, A comparison of four algorithms for change detection in an urban environment. *Remote Sensing of Environment*, **63**, pp. 95–100.

Moser, G. and Serpico, S.B., 2006, Generalized minimum-error thresholding for unsupervised change detection from SAR amplitude imagery. *IEEE Transactions on Geoscience and Remote Sensing*, **44**, pp. 2972–2982.

Otsu, N., 1979, A threshold selection method from gray level histograms. *IEEE Transactions on Systems, Man, and Cybernetics*, **9**, pp. 62–66.

Pajares, G., 2006, A Hopfield neural network for image change detection. *IEEE Transactions on Neural Networks*, **17**, pp. 1250–1264.

Pal, S.K. and Dutta Majumder, D., 1986, *Fuzzy Mathematical Approach to Pattern Recognition* (New York: John Wiley, Halsted Press).

Pal, S.K. and Ghosh, A., 1992a, Fuzzy geometry in image analysis. *Fuzzy Sets and Systems*, **48**, pp. 23–40.

Pal, S.K. and Ghosh, A., 1992b, Image segmentation using fuzzy correlation. *Information Sciences*, **62**, pp. 223–250.

Patra, S., Ghosh, S. and Ghosh, A., 2008, Change detection of remote sensing images with semi-supervised multilayer perceptron. *Fundamenta Informaticae*, **84**, pp. 429–442.

Qiao, Y., Hu, Q., Qian, G., Luo, S. and Nowinski, W.L., 2007, Thresholding based on variance and intensity contrast. *Pattern Recognition*, **40**, pp. 596–608.

Radke, R.J., Andra, S., Al-Kofahi, O. and Roysam, B., 2005, Image change detection algorithms: A systematic survey. *IEEE Transactions on Image Processing*, **14**, pp. 294–307.

Richards, J.A. and Jia, X., 2006, *Remote Sensing Digital Image Analysis*, 4th ed. (Berlin: Springer-Verlag).

Rosenfeld, A., 1984, Fuzzy geometry of image subset. *Pattern Recognition Letters*, **2**, pp. 311–317.

SEZGIN, M. and SANKUR, B., 2004, Survey over image thresholding techniques and quantitative performance evaluation. *Journal of Electronic Imaging*, **13**, pp. 146–165.

SHANNON, C.E., 1948, A mathematical theory of communication. *Bell System Technical Journal*, **27**, pp. 379–423.

SINGH, A., 1989, Digital change detection techniques using remotely sensed data. *International Journal of Remote Sensing*, **10**, pp. 989–1003.

TAO, W.B., TIAN, J.W. and LIU, J., 2003, Image segmentation by three-level thresholding based on maximum fuzzy entropy and genetic algorithm. *Pattern Recognition Letters*, **24**, pp. 3069–3078.

YAGER, R.R., 1979, On the measure of fuzziness and negation, Part I: Membership in the unit interval. *International Journal of General Systems*, **5**, pp. 221–229.

YUAN, F., SAWAYA, K.E., LOEFFELHOLZ, B.C. and BAUER, M.E., 2005, Land cover classification and change analysis of the Twin Cities (Minnesota) metropolitan area by multitemporal Landsat remote sensing. *Remote Sensing of Environment*, **98**, pp. 317–328.

ZADEH, L.A., 1965, Fuzzy sets. *Information and Control*, **8**, pp. 338–353.